J Solid State Electrochem (2009) 13:1181–1191
DOI 10.1007/s10008-008-0638-8

ORIGINAL PAPER

Local electrochemical studies of the microstructural corrosion of AlCu4Mg1 as-cast aluminium alloy and influence of applied strain

H. Krawiec · V. Vignal · Z. Szklarz

Received: 16 May 2008 / Revised: 19 July 2008 / Accepted: 25 July 2008 / Published online: 20 August 2008

Abstract The microstructure of AlCu4Mg1 as-cast aluminium alloy was first determined by means of field emission-scanning electron microscope with an integrated electron dispersion spectrometer, secondary ion mass spectroscopy and atomic force microscopy. Large precipitates (Al_2Cu, Al–Si–Mn–Fe–Cu, oxides) were located at grain boundaries, whereas small particles (aluminium, magnesium and copper) were present in grains. The electrochemical response and pitting susceptibility of sites containing precipitates were then investigated after polishing using the electrochemical microcell technique. After straining, big scattering was observed in the electrochemical response. The most active places corresponded to the sites containing wide microcracks and severe damages in the matrix. In this case, the corrosion potential was around −1,000 mV vs. Ag/AgCl, and the current in the passive domain was five times higher than on the strained matrix. In the absence of severe damage in the matrix or wide microcracks, the corrosion potential was more anodic and the current density in the passive range was around 0.5 mA cm^{-2}. Local polarisation curves carried out in sites containing large precipitates and no defects induced by straining were very close to those obtained in grains far from precipitates.

Keywords Aluminum alloy · Strain · Microstructure · Pitting · Microcracks

H. Krawiec (✉) · Z. Szklarz
AGH University of Science and Technology,
Ul. Reymonta 23,
30-059 Krakow, Poland
e-mail: krawiec@agh.edu.pl

V. Vignal
ICB, UMR 5209 CNRS-Université de Bourgogne,
BP 47870, 21078 Dijon Cedex, France

Introduction

Aluminum alloys are very important category of materials due to their high mechanical properties and wide range of industrial applications, especially in aerospace, automotive and household industries. The mechanical properties of aluminum alloys were developed as a result of heterogeneous microstructures caused by alloying elements and heat treatments. For example, it has been shown [1] that the shearing of strengthening precipitates by dislocations is the prevalent mechanism that controls the plastic deformation of the material. Bypassing of particles, assisted by cross-slip, is an additional process whose effects are enhanced when the temperature increases consistently with the correlated decrease of the flow stress and the hardening rate. This non-planar mechanism leads to a work hardening of the alloy that results in a high mechanical strength. Fracture of aluminum alloys have also been extensively studied using numerical simulation and experimental techniques such as microtomography ([2–4] and references herein).

It is well known [5–7] that aluminum and its alloys are prone to microstructural corrosion (pitting corrosion, intergranual corrosion, etc.). Microstructural corrosion is caused by the presence of intermetallic particles, which may be either anodic or cathodic relative to the matrix [5, 8]. In order to understand the corrosion behavior of aluminum alloys, a comprehensive study on the electrochemical behavior of intermetallic particles that can be present is warranted. Some researchers ([8–12] and references herein) have noted that the compounds containing Cu, Fe and Ti are generally more noble than pure aluminum or the matrix analog and that compounds like Al_3Fe, Al_7Cu_2Fe, Al_2Cu and Al_3Ti reveal a characteristic breakdown potential, suggesting that they are capable of maintaining a passive film. By contrast, intermetallics

containing Mg, Zn and Si are less noble than pure Al or the matrix analog, and the intermetallic compounds like $Al_{32}Zn_{49}$, $MgZn_2$ and Mg_2Si do not show the breakdown potential, and they are capable of corroding freely above corrosion potential.

Numerous studies have been devoted to understand stress corrosion cracking processes in aluminium alloys [13–15]. By contrast, limited research has been performed to investigate the influence of mechanical stress on pitting corrosion processes. Potentiodynamic polarisation measurements in 1 M NaCl indicated that the two breakdown potentials typically observed for AA2024-T3 were lower on stressed samples, and the current at a given potential was higher [16]. On the other hand, electrochemical measurements on AA2024-T3 supported the findings of the beneficial effects of compression on localised corrosion. The breakdown and repassivation potentials increased, and passive current density decreased for samples under compression or with compressive residual stress [17].

In this paper, the microstructure of AlCu4Mg1 as-cast aluminium alloy was first determined by means of field emission–scanning electron microscope with an integrated electron dispersion spectrometer (FE-SEM/EDS), secondary ion mass spectroscopy (SIMS) and atomic force microscopy (AFM). The electrochemical response of sites containing metallurgical (precipitates…) and mechanical (microcracks, rough surfaces…) heterogeneities was studied at the microscale using the electrochemical microcell technique. In order to investigate the behavior of all the sites of interest, microcapillaries in the range of 5–30 μm were used. Mechanical criteria leading to significant increase of the pitting susceptibility of the material were proposed.

Experimental

Materials, specimens and surface preparation

Experiments were performed on AlCu4Mg1 as-cast aluminium alloy (chemical composition, wt.%; Cu, 4.437; Fe, 0.205; Mn, 0.854; Zn, 0.067; Mg, 0.551; Si, 0.47; Ni, 0.005; Ti, 0.019; Sn, 0.009; Cr, 0.023; Pb, 0.012; Zr, 0.002; Al, 93.35). Microstructural and electrochemical investigations were first performed on plates (2-mm thickness, 23-mm width and 27-mm length). The role of mechanical strain was then investigated on tensile specimens (gauge surface, 35×5 mm^2). Both sets of specimens were mechanically polished with silicon carbide (SiC) papers down to 4,000 grit and diamond pastes (9, 3 and 1 μm). They were smoothed using colloidal silica. Between each step, specimens were ultrasonically cleaned in ethanol.

Electrochemical measurements at the microscale

The local electrochemical behavior of specimens was studied in 0.1 M NaCl solution at room temperature using the electrochemical microcell technique. This technique consists of a glass micro-capillary that is filled with electrolyte. The micro-capillary tip was sealed to the specimen surface with a layer of silicon rubber. The microcell was mounted on a microscope for precise positioning of the micro-capillary on the surface. The diameter of the micro-capillary tip was in the range of 5–30 μm, depending on the microstructure to be studied. The counter electrode was a platinum wire, and the reference electrode was Ag/AgCl. A modified high-resolution potentiostat was used in order to have a current detection of about 20 fA. The potentiodynamic polarisation curves were determined from −1,500 mV vs. Ag/AgCl to the anodic direction at various potential scan rates (16.6 and 1 mV s^{-1}). The current was low-pass filtered (cutoff frequency, 20 Hz). Note that no prior polarisation in the cathodic domain was applied to the system.

Surface observations and chemical analyses at the microscale

A field-emission-type scanning electron microscope (JEOL 6400F) with an integrated electron dispersion spectrometer (FE-SEM/EDS) was used to determine the morphology and the chemical composition of precipitates. 3D images of the specimen surface were obtained from AFM (Q-Scope 350 from Quesant Instrument Corporation). AFM images were acquired in contact mode, and they were analysed using the Q-analysis 4.0 software package.

The chemical composition of precipitates and the matrix close to the surface was investigated from SIMS. These measurements were performed using a MIQ 256 Cameca Riber apparatus located in an ultra-high vacuum chamber (of about 3.3×10^{-7} Pa). Repartition of $^{24}Mg^+$, $^{30}Si^+$, $^{63}Cu^+$ and $^{43}AlO^+$ ions on sites containing precipitates was obtained using an Ar^+ primary ion source (10 keV, incident angle of 45°). Surface scanning was 95×134 μm^2 with magnification ×3,000. Acquisition of the images (128×128 pixels) was performed without preliminary sputtering and by applying a current of 5 nA and dwell time of 3.66×10^{-3} s per pixel.

Results and discussion

Microstructure of specimens after polishing

The microstructure of AlCu4Mg1 specimens and the chemical composition of precipitates were first studied at

the microscale by means of FE-SEM/EDS, SIMS, AFM and optical microscopy. Both large and small precipitates were observed at the specimen surface, as shown in Fig. 1. FE-SEM observations revealed that large precipitates were systematically located at grain boundaries of the matrix (Fig. 1a). They were composed of Al_2Cu (Al, 64.43±0.2 at. %, and Cu, 35.56±0.2 at.%) or Al–Si–Mn–Fe–Cu (Al, 69.52±0.4 at.%; Si, 8.72±0.16 at.%; Mn, 8.25±0.23 at.%; Cu, 6.87±0.28 at.% and Fe, 6.62±0.2 at.%). Chemical analysis was carried out over a large number of precipitates, and a small scatter in the content of alloying elements was found, indicating that such precipitates have a homogeneous composition. Note that it was possible to distinguish these two types of large precipitates by means of optical microscopy (used to select the sites of interest in microelectrochemistry). AFM images obtained in air show that large precipitates were higher than the matrix after mechanical polishing. The height difference was about 50 nm. In addition, no microvoids were detected at the interface between large precipitates and the metallic matrix.

Oxide precipitates were also detected at grain boundaries, as shown in Fig. 1b. They were mainly composed of oxygen, aluminium and copper, as reported in Table 1. A small amount of magnesium and silicon was also detected in some of them. Six oxides were analysed, and a large scatter in the content of alloying elements was obtained (between 2 and 30 wt.% for copper in Table 1, for instance), indicating that they have non-homogeneous composition.

Surface observations at high resolution revealed the presence of small particles in metallic grains, as shown in Fig. 1b–d. They were elongated, with a length in the range of 1–2 μm and a width of about 0.3 μm. The matrix surrounding large precipitates and the majority of small grains were free of such metallurgical heterogeneities. Comparing the chemical composition of sites in the matrix free of any metallurgical heterogeneities (sites 1–3 in Fig. 1c and values in Table 2) and sites containing small particles (sites 4–6 in Fig. 1c and values in Table 2) indicates that small particles are enriched in copper and magnesium. FE-SEM/EDS measurements carried out in the same particle (sites 7–9 in Fig. 1d, values reported in Table 2) confirm that they are homogeneously composed of copper, aluminium and a small amount of magnesium.

Surface distribution of copper, silicon and magnesium in a site containing Al_2Cu precipitates (Fig. 2a) was then investigated from SIMS experiments. The results are shown in Fig. 2b–e. Note that the repartition of iron and manganese could not be determined because their signals overlap. These experiments confirm that copper was mainly found in precipitates (SIMS intensity greater than 80 a.u. in Fig. 2b). Furthermore, copper was more or less uniformly distributed in the matrix close to the large precipitates (where no small precipitates were found by means of FE-SEM/EDS) and also in small precipitates (SIMS intensity in the range of 50–80 a.u. in Fig. 2c). Magnesium was also found in very small quantities at the surface of large precipitates. On the other hand, the matrix contains a small

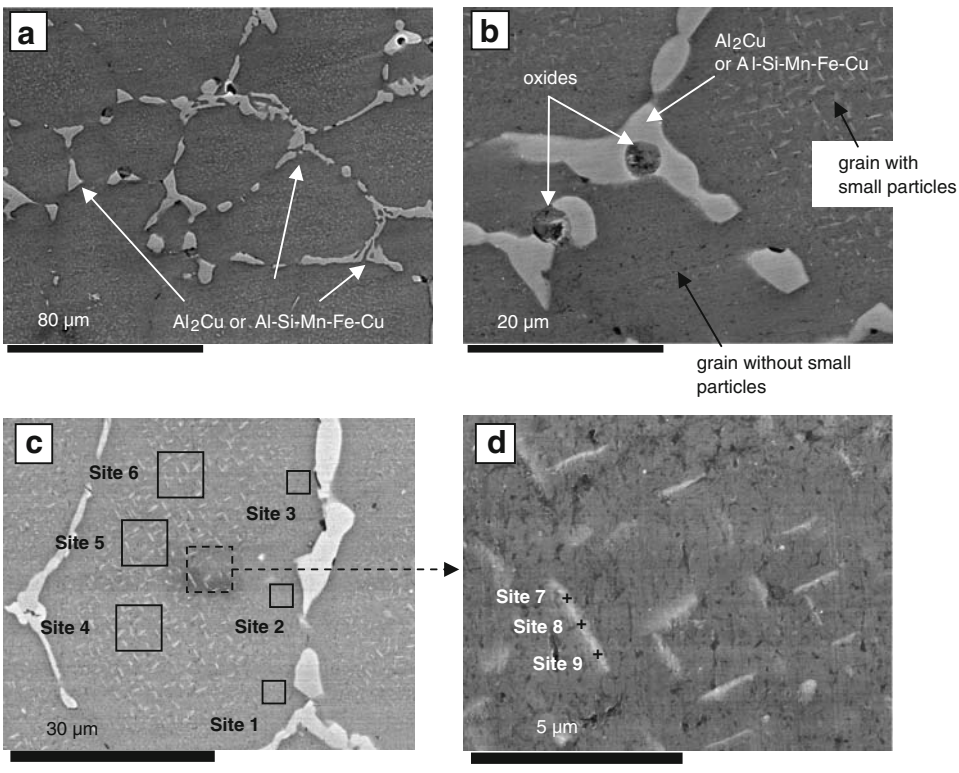

Fig. 1 a–d SEM micrographs of the specimen microstructure after polishing

Table 1 Chemical composition (wt.%) of several oxide precipitates determined by means of FE-SEM/EDS

	Al	Cu	Mg	Si	O
Oxide 1	84.54	2.55	0.79	3.22	8.9
Oxide 2	45.25	27.12	1.2	9.41	17.02
Oxide 3	62.38	18.23	0.9	2.19	16.3
Oxide 4	66.83	26.22	–	0.73	6.21
Oxide 5	31.46	29.41	–	–	39.13
Oxide 6	67.41	13.99	–	1.45	17.14

amount of copper (SIMS intensity in the range of 25–50 a.u.) and magnesium (SIMS intensity in the range of 35–65 a.u.), corresponding to α-Al matrix phase (Al–Cu solid solution).

Electrochemical behavior of polished specimens in 0.1 M NaCl

Local polarisation curves were first plotted on sites located far from large precipitates using the electrochemical microcell technique and 25-µm microcapillaries. The potential scan rate was set at 16.6 mV s^{-1} (green curves in Fig. 3a). The corrosion and pitting potentials of such sites, which contain both small particles and the metallic matrix, were −660 and −120 mV vs. Ag/AgCl, whereas the current density in the passive range was 0.1 mA cm^{-2}. A similar electrochemical response was obtained using extremely small microcapillaries (diameters in the range of 5–10 µm, black curves in Fig. 3a). Scattering in the pitting potential values (between −250 and 0 mV vs. Ag/AgCl) was found, indicating that the matrix has heterogeneous electrochemical behavior at the microscale. These values were, however, centered on the value obtained using 25-µm microcapillaries. By contrast, lower cathodic current densities were measured in small grains (grey curves in Fig. 3a). It was previously shown that these grains have no small particles and are depleted in copper.

The potential scan rate was then set at 1 mV s^{-1}. In this case, the potential was applied in the cathodic domain for 1,200 s (instead of 50 s at a potential scan rate of 16.6 mV s^{-1}). Considering the current densities reached (Fig. 3b), a large quantity of dissolved oxygen was reduced, leading to a significant increase of the pH close to the specimen surface. As it was observed in the case of stainless steels [18], pH values around 9 may be reached. Under these conditions, aluminum oxide Al_2O_3 was unstable and an activation peak was observed at −220 mV vs. Ag/AgCl on polarisation curves (Fig. 3b). The maximum current density in the peak was roughly 0.3 and 0.15 mA cm^{-2} in sites located far from precipitates (large grains) and in small grains, respectively. In addition, pitting potential was found to be much higher in the latter case (of about 800 mV vs. Ag/AgCl) than in the former case (of about 430 mV vs. Ag/AgCl). These differences could be related to the presence of small particles in large grains, but additional experiments are necessary to confirm such an assumption.

The electrochemical response of the matrix with different types of precipitates was determined after polishing using 25-µm microcapillaries, as shown in Fig. 4. The cathodic current measured on sites containing Al_2Cu precipitates was higher than on the matrix, leading to a shift of the corrosion potential of about 130 mV vs. Ag/AgCl in the anodic direction (Fig. 4a). This confirms that copper enhances cathodic reactions. Stable pits initiated within the same potential range as on the metallic matrix (of about −115 mV vs. Ag/AgCl), suggesting that pits initiate in the surrounding grains. By contrast, pitting potential was significantly lower on sites containing oxides (values below −150 mV vs. Ag/AgCl instead of −115 mV vs. Ag/AgCl in the matrix), indicating that oxides constitute precursor sites for pitting corrosion (Fig. 4b). Local polarisation curves determined on sites containing Al–Si–Mn–Fe–Cu precipitates showed no differences from those obtained on the matrix, both in the cathodic and anodic domains (Fig. 4c).

To identify precursor sites around Al–Si–Mn–Fe–Cu precipitates, surface observations were performed after microelectrochemical test using FE-SEM/EDS and AFM, as shown in Fig. 5a and b. The precipitate surface (site 1 in Fig. 5, chemical composition in Table 3) remained smooth, and no pores were observed at high resolution. In addition, the height difference between the matrix and the precipitate was again 50 nm (Fig. 5c), indicating that no localised dissolution (or selective dissolution) of the precipitate occurred. A high density of corrosion products was observed around the precipitate (sites 2–8, chemical composition in Table 3). Note that the main pit was located in the close vicinity of the precipitate/matrix interface (site 2).

Table 2 Chemical composition (at.%) of various sites reported in Fig. 1 determined by means of FE-SEM/EDS

	Al	Cu	Mg
Site 1 in matrix	98.22	1.26	0.53
Site 2 in matrix	98.10	1.55	0.35
Site 3 in matrix	98.22	1.34	0.44
Site 4 in matrix + small particles	97.6	1.79	0.62
Site 5 in matrix + small particles	96.7	2.7	0.61
Site 6 in matrix + small particles	97.47	1.97	0.61
Site 7 in small particle	91.44	7.74	0.81
Site 8 in small particle	91.66	8.06	0.28
Site 9 in small particle	91.54	8.11	0.35

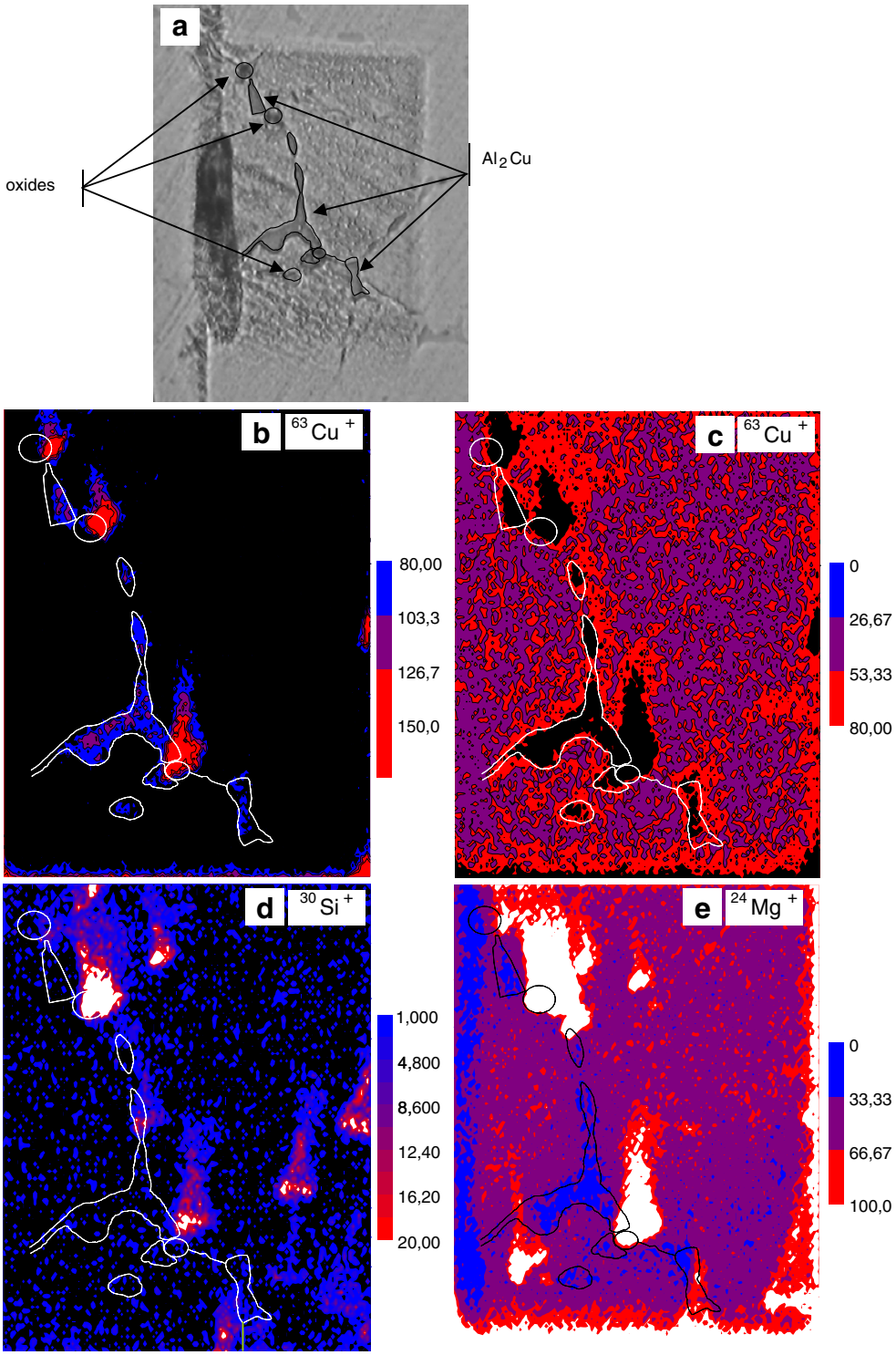

Fig. 2 **a** Optical micrograph of Al_2Cu and oxide precipitates after polishing. Repartition of ionic species around these precipitates from SIMS using Ar^+ primary ions: **b** and **c** high- and low-signal ranges of copper, **d** full signal range of silicon and **e** full-signal range of magnesium

Mechanical behaviour of specimens under straining conditions

No microcracks were detected at the specimen surface after 2% plastic strain. By contrast, numerous microcracks propagating perpendicularly to the loading direction were observed in both types of precipitates (namely Al_2Cu, Al–Si–Mn–Fe–Cu and oxides) after 4% plastic strain, as shown in Fig. 6a. Note that microcracks could be more than 1-μm wide in some places (Fig. 6b), and such surface defects may have significant impact on the corrosion behaviour of strained specimens. Microcracks were also observed at the interface between precipitates and the metallic matrix, as shown in Fig. 6c and d. In addition,

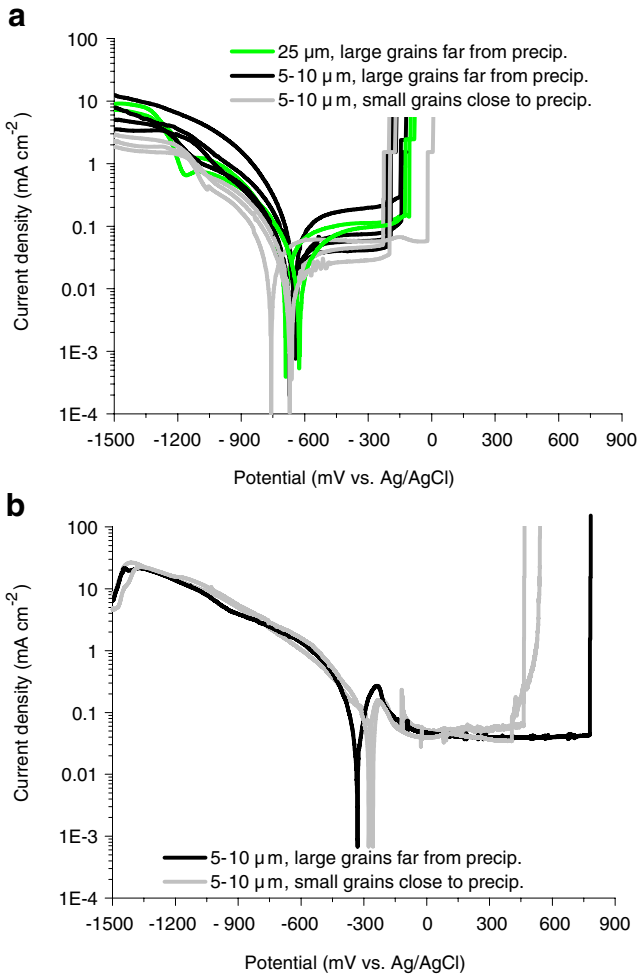

Fig. 3 Local polarisation curves determined on sites of polished specimens containing the matrix at a potential scan rate of **a** 16.6 mV s^{-1} and **b** 1 mV s^{-1}. The microcapillary diameters used are reported in the figures

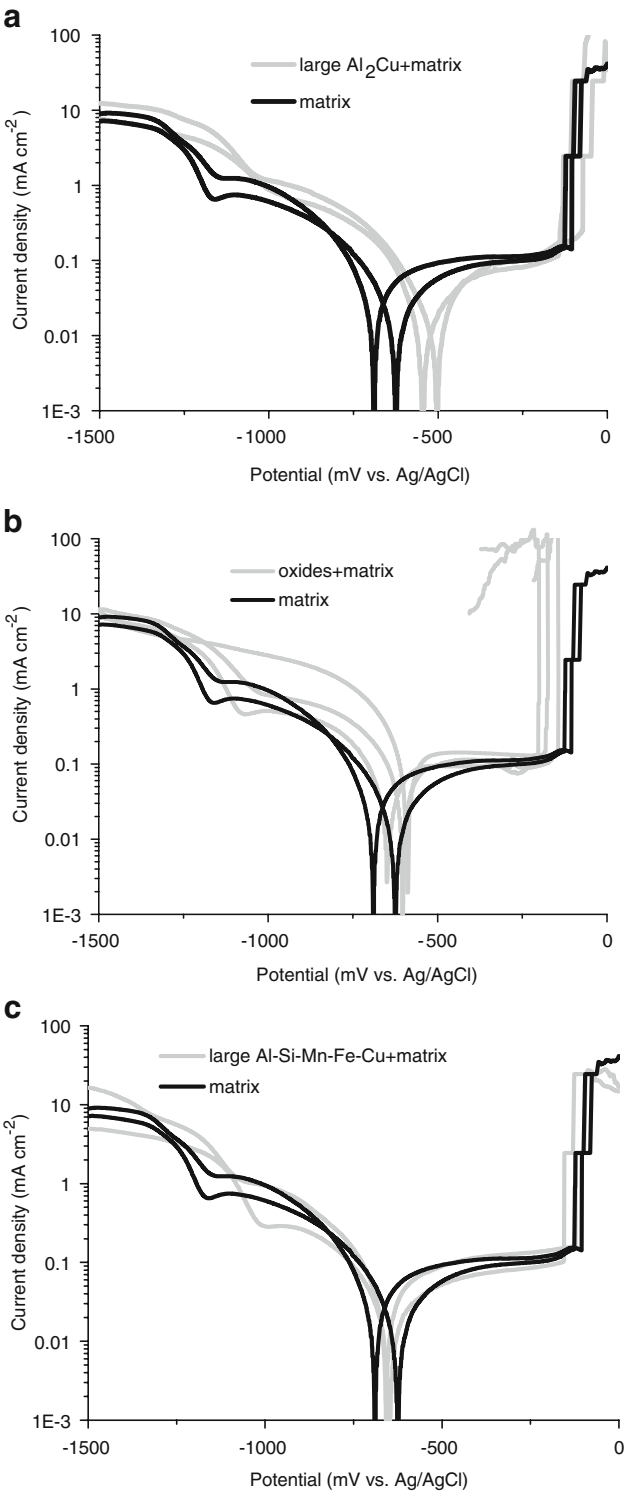

Fig. 4 Local polarisation curves (potential scan rate of 16.6 mV s^{-1}, 25-µm microcapillaries) determined on sites of polished specimens containing the matrix and precipitates: **a** Al_2Cu, **b** oxides and **c** Al–Si–Mn–Fe–Cu

strain concentrations were developed at the tip of microcracks, leading to some damages in the metallic matrix, as shown in Fig. 6e. In some cases, microcracks propagated along grain boundaries, between two large precipitates, as shown in Fig. 6f. After 5.5% plastic strain, the density of microcracks in precipitates, along the matrix/precipitate interfaces and grain boundaries increased significantly (Fig. 7). Microcrack opening was often detected at this strain level, leading to very wide defects, such as those in Fig. 7a.

Electrochemical behaviour of strained specimens in 0.1 M NaCl

Local electrochemical measurements were first performed on the matrix after 5.5% plastic strain, as shown in Fig. 8a. Note that 30-µm microcapillaries were used. Contrary to the polished surface (green curves in Fig. 3a), big scattering

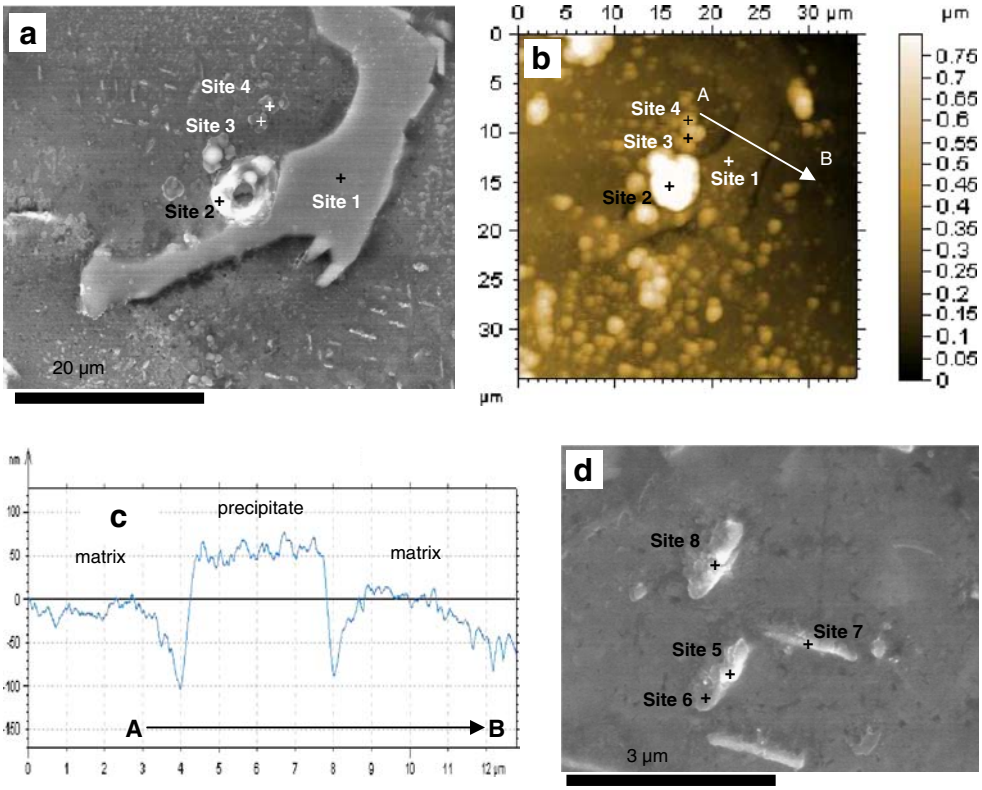

Fig. 5 **a** SEM and **b** AFM images of a site containing an Al–Si–Mn–Fe–Cu precipitate after local corrosion test performed in 0.1 M NaCl using the electrochemical microcell technique. **c** Profile section along the line A–B visible in **b**. **d** SEM image of the matrix and small particles after local corrosion test

in the results was obtained, indicating that the strained surface is highly heterogeneous. The corrosion potential was located between −1,000 and −850 mV vs. Ag/AgCl, whereas the pitting potential was in the range of −380/−200 mV vs. Ag/AgCl. Therefore, these two parameters were significantly shifted to the cathodic direction after straining. In addition, the current density in the passive domain reached values around 0.17 mA cm^{-2} in some grains (instead of 0.1 mA cm^{-2} on the polished specimen). This indicates that the surface of aluminium alloys strained in the plastic domain is more active than after polishing. Experiments performed using extremely small microcapillaries show that both sites far from large precipitates and sites in small grains surrounded by precipitates are more active after straining (Fig. 8b). For instance, the pitting potential is between 0 and −150 mV vs. Ag/AgCl (Fig. 8b) instead of between 450 and 800 mV vs. Ag/AgCl on the polished surface (Fig. 3b).

Big scattering was also observed in the electrochemical response of sites containing large precipitates with microcracks, as shown in Fig. 9a. The most active places were found to correspond to the sites containing wide microcracks and severe damages in the surrounding matrix (Fig. 9b). In this case, the corrosion potential was around −1,000 mV vs. Ag/AgCl, and the current in the passive domain was 0.9 mA cm^{-2} (five times higher than on the pure matrix after straining). In the absence of severe damages in the matrix (Fig. 9c) and/or wide microcracks (Fig. 9d), the corrosion potential was more anodic, and the current density in the passive range was around 0.5 mA cm^{-2}. Local polarisation curves carried out in sites containing a large precipitate and no surface defects

Table 3 Chemical composition (wt.%) of various sites reported in Fig. 5 determined by means of FE-SEM/EDS

	O	Mg	Al	Si	Cl	Mn	Fe	Cu
Site 1 in precipitate	2.28	–	53.97	7.04	–	13.40	11.91	11.41
Site 2 in corrosion product	4.74	–	57.39	5.55	–	12.82	10.67	8.84
Site 3 in corrosion product	11.06	0.58	82.80	0.35	0.90	0.76	0.52	3.02
Site 4 in corrosion product	8.92	–	86.00	0.18	0.82	0.70	0.75	2.64
Site 5 in corrosion product	7.11	0.46	80.91	–	–	1.04		10.49
Site 6 in corrosion product	7.84	0.42	83.50	0.40	–	0.62		7.23
Site 7 in corrosion product	7.35	0.44	84.00	–	–	0.70		7.51
Site 8 in corrosion product	8.50	0.72	81.01	0.75	0.48	0.96		7.58

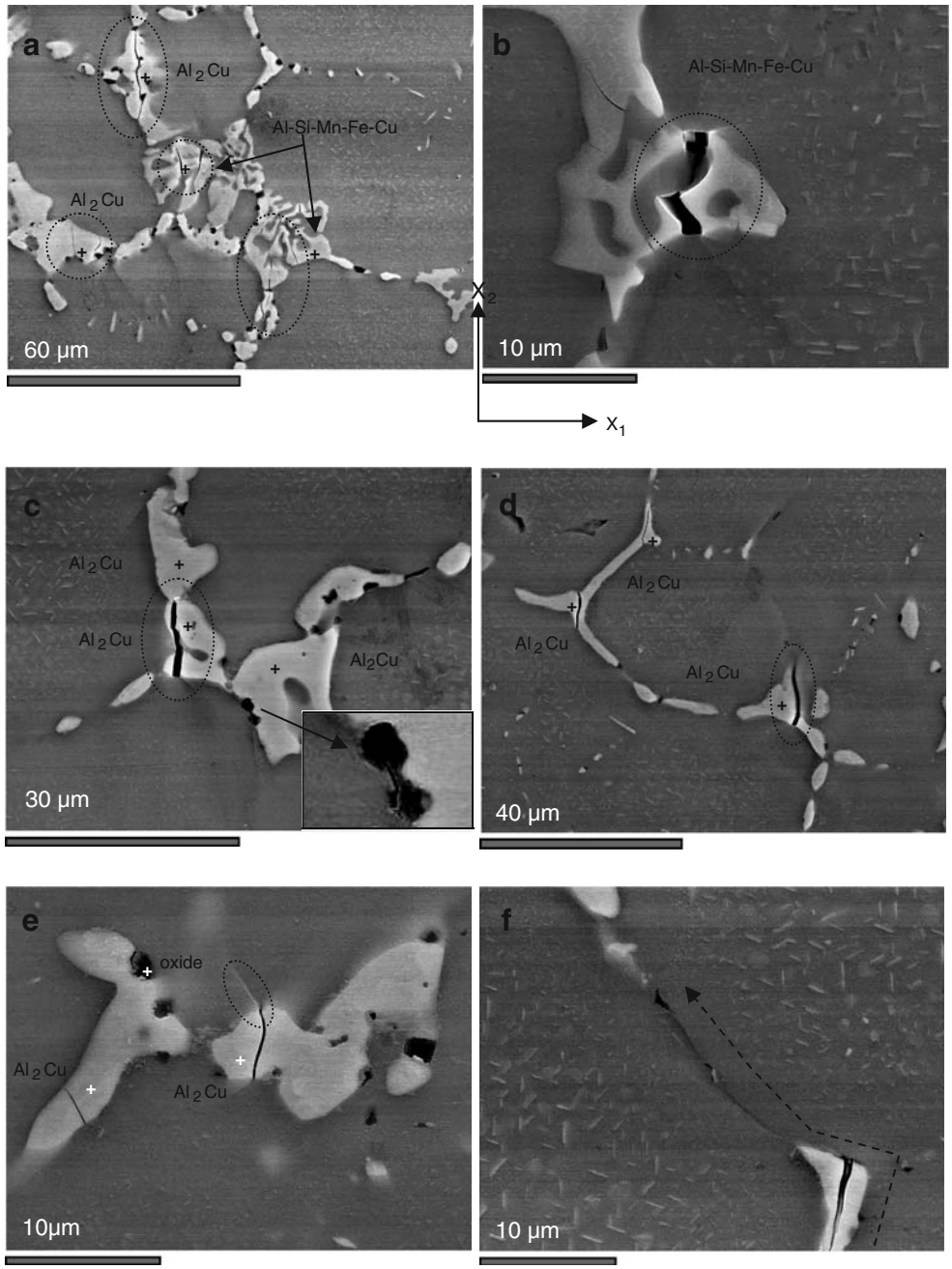

Fig. 6 SEM micrographs of strained specimens (4% plastic strain applied along the X_1-axis) showing microcracks **a** and **b** in large precipitates, **c** and **d** along the precipitate/matrix interface and **e** and **f** in the matrix along a grain boundary

induced by straining (microcracks or damages in the matrix, grey curve in Fig. 9e) were very close to those obtained in grains far from precipitates (Fig. 8a).

Discussion

Surface observations of AlCu4Mg1 as-cast aluminium alloy have shown the presence of large Al_2Cu and Al–Si–Mn–Fe–Cu precipitates with their associated precipitate free zones (PFZ) at grain boundaries and small Al–Cu–Mg precipitates in large metallic grains. PFZs can form as a result of solute depletion caused by the solute diffusing towards and along the high diffusivity pathways (interfaces, defects and grain boundaries) or by vacancy depletion due to vacancy annihilation at the interfaces and defects.

Regarding the corrosion behaviour of aluminium alloys, authors usually refer to a galvanic coupling phenomenon between the particles and the surrounding matrix. Considering a simple Al/Cu system, it has been shown [19] that

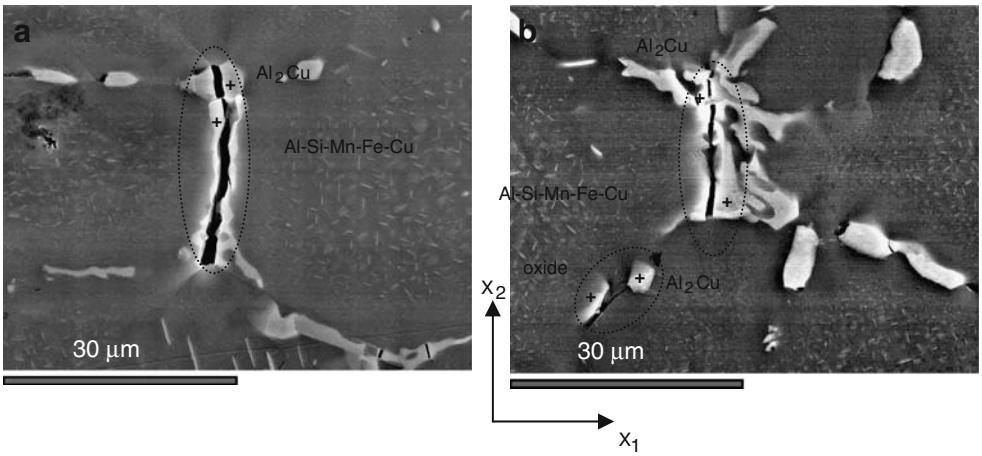

Fig. 7 **a** and **b** SEM micrographs of strained specimens (5.5% plastic strain applied along the X_1-axis) showing microcracks in precipitates and along grain boundaries in the matrix

the reaction occurring at the copper electrode is oxygen reduction. This leads to a local pH increase. Values higher than 9 can be reached, allowing the dissolution of aluminium to occur close to the interface. In the present study, similar damages were observed around Al_2Cu and Al–Si–Mn–Fe–Cu precipitates (Fig. 5a and b). In the case of Al_2CuMg immersed in chloride-containing solutions at OCP, a three-step mechanism has been proposed [20], corresponding to (1) preferential dissolution of Al and Mg, (2) galvanic coupling between the Cu-enriched particles and the surrounding matrix and (3) Cu deposition around the corroded particles. SEM observations on small corroded particles of AlCu4Mg1 as-cast aluminium alloy also indicate that the particles are dissolved and covered by corrosion products, whereas the surrounding matrix is intact (Fig. 5d).

Due to differences in mechanical properties between the matrix, the PFZ and precipitates, heterogeneous strain fields are expected to be developed at the specimen surface under straining conditions. It has been suggested ([21] and references herein) that, when strains in the PFZ rise beyond a critical value, typically around 0.5 for the relatively weak PFZ, failure occurs in the PFZ. High strain levels reached in the plastic zone around the crack tip are often sufficient to break locally precipitates. The ultimate strength (UTS) of Al_2Cu has been assessed through comparison of observations on fractured and intact particles close to a crack tip and finite element modelling of the stresses in this region [2, 22–23]. The UTS was found to be more or less independent of their shape and size (in the range of 5–16 µm), and a mean value of 700 MPa was proposed. By contrast, no data are available for Al–Si–Mn–Fe–Cu precipitates. Such a mechanism may explain initiation of micro-cracks at large precipitates in AlCu4Mg1 as-cast aluminium alloy. However, a full understanding of fracture behaviour and fracture/microstructure interaction in AlCu4Mg1 as-cast aluminium alloy (initiation of micro-cracks in the precipitate itself or in the PFZ, etc.) requires future investigations at the nanoscale. Numerical simulation based on a shear lag model approach [21] was validated from the experimental data described previously and permitted to demonstrate that particles with sizes below

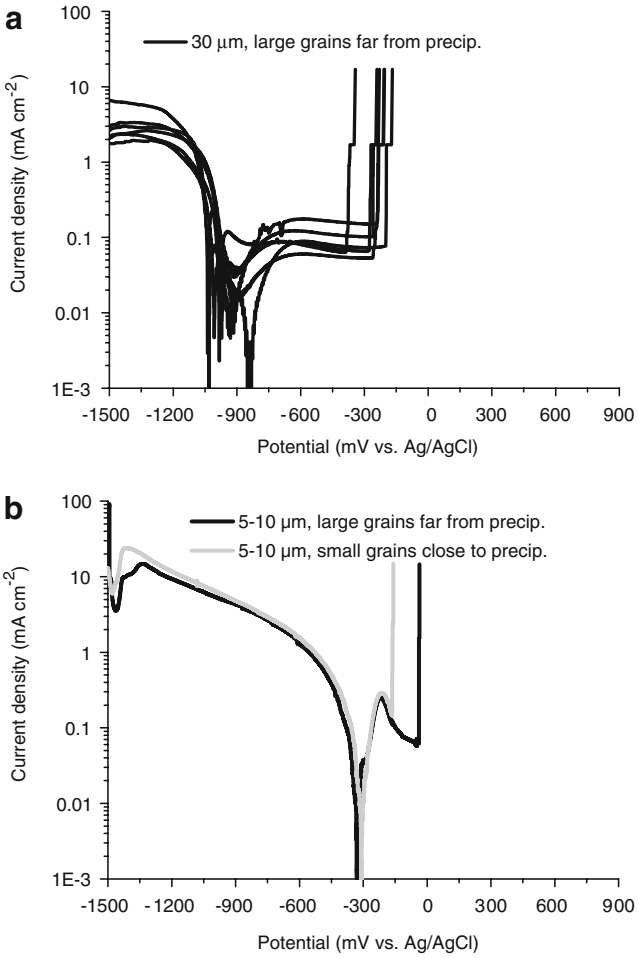

Fig. 8 Local polarisation curves determined on sites of strained specimens containing the matrix at a potential scan rate of **a** 16.6 mV s^{-1} and **b** 1 mV s^{-1}

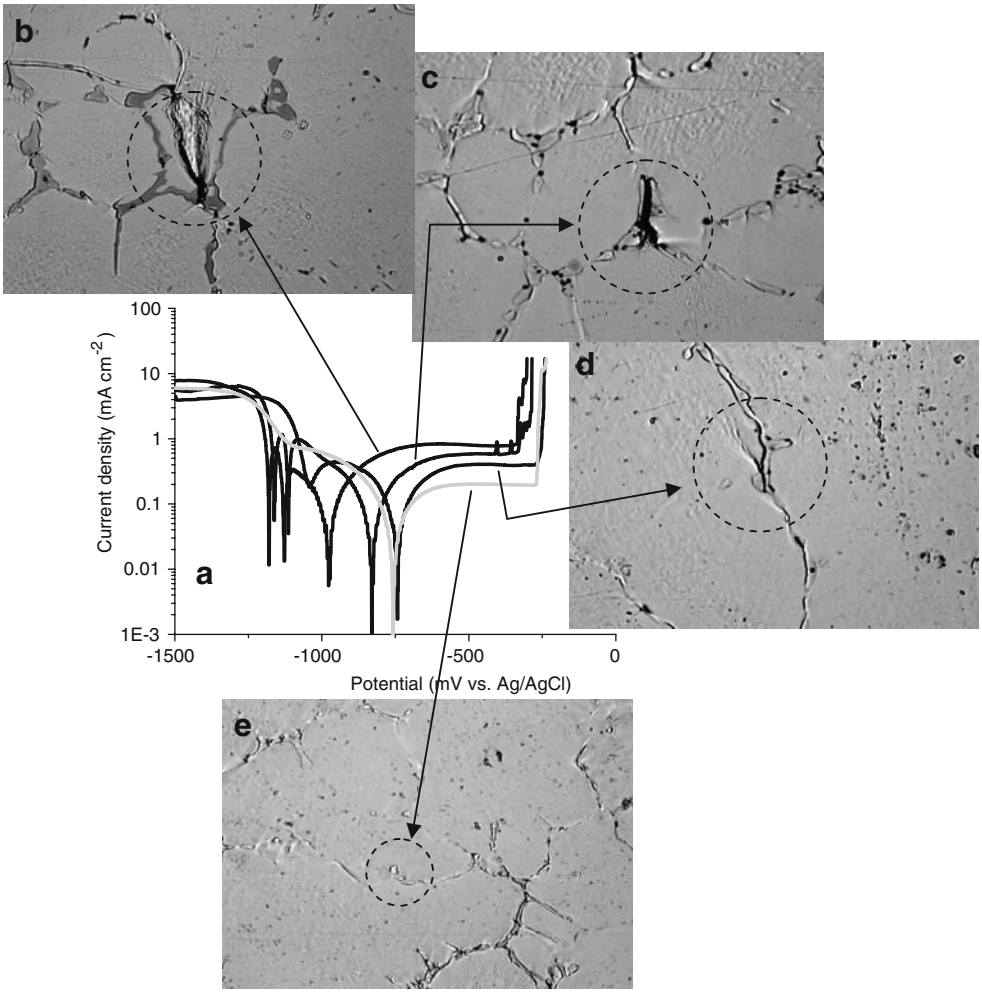

Fig. 9 **a** Local polarisation curves (potential scan rate of 16.6 mV s^{-1}, 30-µm microcapillaries) determined on sites of strained specimens containing the matrix with precipitates and microcracks. **b**–**e** Optical micrographs where local measurements were performed

2 µm, such as those observed in metallic grains of AlCu4Mg1 as-cast aluminium alloy, do not break.

Applied strain was found to modify systematically the corrosion behaviour of AlCu4Mg1 as-cast aluminium alloy. In the presence of a stable native oxide film, pitting potential was slightly decreased and values around −240 mV vs. Ag/AgCl were found after straining (Fig. 8a) instead of −120 mV vs. Ag/AgCl after polishing (green curves in Fig. 3a). One may assume that the diffusivity of anions into the oxide film was increased, according to a mechanism similar to that proposed for protons [24]. In the presence of a newly formed oxide film, pitting potential drops from values in the range of 400–800 mV vs. Ag/AgCl on the polished surface (Fig. 3b) down to values between −150 and −50 mV vs. Ag/AgCl on the strained specimens (Fig. 8b). One may assume that the structure and/or the chemical composition of the oxide film growing on the strained surface are strongly affected by deformation processes, increasing drastically the corrosion susceptibility of the material.

Conclusions

The microstructure of AlCu4Mg1 as-cast aluminium alloy was first determined by means of FE-SEM/EDS, SIMS and AFM. Large precipitates (composed of Al_2Cu, Al–Si–Mn–Fe–Cu and oxides) were systematically located at grain boundaries, whereas small particles (containing aluminium, magnesium and copper) were present in some metallic grains. The electrochemical response and pitting susceptibility of sites containing precipitates were then investigated after polishing using the electrochemical microcell technique. Experimental results were reproducible, and it was both shown that oxides constitute precursor sites for pitting corrosion and cathodic reactions were promoted on copper-enriched particles.

Big scattering was observed in the electrochemical response of strained specimens. The most active places were found to correspond to the sites containing wide microcracks and severe damages in the matrix. In this case, the corrosion potential was around −1,000 mV vs. Ag/

AgCl, and the current density in the passive domain was around 1 mA cm^{-2} (five times higher than on the strained matrix). In the absence of severe damage in the matrix or wide microcracks, the corrosion potential was more anodic and the current density in the passive range was around 0.5 mA cm^{-2}. Local polarisation curves carried out in sites containing large precipitates and no defects induced by straining were very close to those obtained in grains far from precipitates.

Acknowledgment This work was supported by the French–Polish bilateral program Polonium (project no. 17798ZH) and Polish Ministry of Science and Higher Education (grant N507 no. 28.28.170.7004). The authors would like to thank Dr. O. Heintz (ICB) for assistance in SIMS experiments and Dr. C. Josse (ICB) for assistance in FE-SEM/EDS observations.

References

1. Delmas F, Vivas M, Lours P, Casanove MJ, Couret A, Coujou A (2003) Mater Sci Eng A 340:286
2. Kobayashi T (2000) Mater Sci Eng A 286:333
3. Qian L, Toda H, Uesugi K, Ohgaki T, Kobayashi M, Kobayashi T (2008) Mater Sci Eng A 483–484:293
4. Toda H, Sinclair I, Buffiere JY, Maire E, Khor KH, Gregson P, Kobayashi T (2004) Acta Mater 52:1305
5. Nisancioglu K (1990) J Electrochem Soc 137:69
6. Mc.Cafferty E (2003) J Electrochem Soc 150:B238
7. Searles JL, Gouma PI, Buchheit RG (2001) Metall Mater Trans A 32:2859
8. Birbilis N, Buchheit RG (2005) J Electrochem Soc 152:B140
9. Guillaumin V, Mankowski G (1999) Corr Sci 41:421
10. Campestrini P, van Westing EPM, van Rooijen HW, de wit JHW (2000) Corr Sci 42:1853
11. Little DA, Connolly BJ, Scully JR (2007) Corr Sci 49:347
12. Ambat R, Davenport AJ, Scamans GM, Afseth A (2006) Corr Sci 48:3455
13. Vogt H, Speidel MO (1998) Corr Sci 40:251
14. Lin CK, Yang ST (1998) Eng Fract Mech 59:779
15. Dymek S, Dollar M (2003) Mater Chem Phys 81:286
16. Liu X, Frankel GS, Zoofan B, Rokhlin SI (2004) Corr Sci 46:405
17. Liu X, Frankel GS (2006) Corr Sci 48:3309
18. Webb EG, Alkire RC (2002) J Electrochem Soc 149:B280
19. Jorcin JB, Blanc C, Pebere N, Tribollet B, Vivier V (2008) J Electrochem Soc 155:C46
20. Lacroix L, Ressier L, Blanc C, Mankowski G (2008) J Electrochem Soc 155:C131
21. Starink MJ (2005) Mater Sci Eng A 390:260
22. Kobayashi T (2003) Mater Sci Forum 426:67
23. Toda H, Kobayashi T, Takahashi A (1999) Alum Trans 1:109
24. Beck W, Bockris JO'M, McBreen J, Nanis L (1966) Proc R Soc A290:220